*Supporting information for Nano Letters*

# Inorganic Nanoshell-Stabilized Liquid Metal for Targeted Photo-Nanomedicine in NIR-II Biowindow

*Piao Zhu,[1,2] Shanshan Gao,[1,2] Han Lin,[1,2] Xiangyu Lu,[1,2] Bowen Yang,[1,2] Linlin Zhang,[1] Yu Chen[1*] and Jianlin Shi[1*]*

[1]The State Key Lab of High Performance Ceramics and Superfine Microstructure, Shanghai Institute of Ceramics, Chinese Academy of Sciences, Shanghai 200050, P. R. China.

[2]University of Chinese Academy of Sciences, Beijing 100049, P. R. China.

E-mail: chenyu@mail.sic.ac.cn (Y. Chen), phone number: 021-52412018, fax number: 86-21-52413903; jlshi@mail.sic.ac.cn (J. Shi), phone number: 021-52412712, fax number: 86-21-52413903.

## *Table of Contents*

**Part A.** Supplementary experimental details

**Part B.** Supplementary figures and discussions

**Part C.** Supplementary tables

**Part D.** References

## *Part A. Supplementary experimental details*

### 1. Materials and Reagents

Tetraethyl orthosilicate (TEOS), ammonia solution (30 %) and ethanol were obtained from Sinopharm Chemical Reagent Co., Ltd (Shanghai, China). Liquid metal (EGaIn, 75 % Ga and 25 % In by weight), (3-Aminopropyltriethoxysilane (APTES), N-hydroxysuccinimide (NHS), N-(3-(dimethylamino) propyl)-N'-ethylcarbodiimide hydrochloride (EDC) and Fluorescein isothiocyanate (FITC) was purchased from Sigma-Aldrich. Bis(γ-triethoxysilylproyl)tetrsulfide (BTES) and 3-mercaptopropyltriethoxysilane (MPTES) were obtained from Shanghai Aladdin Biochemical Technology Co., Ltd. Maleimide PEG NHS Ester (MAL-$PEG_{2000}$-SCM) and Methoxy PEG silane (M-SLN-2000) was purchased from Jenkem Technology Co., Ltd. Cell Counting Kit-8 (CCK-8) and phosphate buffer solution (PBS) were bought from Shanghai Ruicheng BioTech Co., Ltd. DAPI staining solution was bought from Beyotime Biotechnology. RGD peptides were purchased from Chinese Peptide Company. Annexin V, FITC Apoptosis Detection Kit (50assays), 3,8-diamino-5-[3-(diethylmethylammonio)propyl]-6-phenylphenanthridinium diiodide (PI), 3,6-di(O-acetyl)-4,5-bis[N,N-bis(carboxymethyl)aminomethyl]fluorescein, tetraacetoxymethyl ester (Calcein-AM) were purchased from Dojindo Molecular Technologies, Inc. Deionized water was used in all experiments. All chemicals were used as received without further purification.

### 2. Synthesis of liquid metal@$SiO_2$-RGD nanoparticles.

**a. Synthesis of liquid metal nanoparticles:** The liquid metal nanoparticles were synthesized by transferring 100 μL liquid metal (EGaIn) to 10 mL alcohol in the glove-box. After immersing the high-intensity ultrasonic titanium horn-type sonicator, the opening between the bottle and transducer microtip was covered with Parafilm as completely as possible in tandem. And then the EGaIn was under probe sonication with an ultrasonic transducer for 2 h at the power of 400 W in a 20 ℃ oil bath. The ultrasound probe worked 5 s with the interval of 5 s.

**b. Deposition of the $SiO_2$ protective layer:** 10 mL 7 % diluted $NH_3 \cdot H_2O$ was added into the 20 mL EGaIn slurry diluted with water to make a weak alkaline environment for the hydrolysis of silicon sources. Accelerated by the acoustic cavitation effect, a thin $SiO_2$ layer was deposited on

the inert $Ga_2O_3$ layer by 5 mL 10 % silicon sources-ethanol solution injected by springe pump at an injection rate of 2 $mL \cdot h^{-1}$ after 4 h sonication in a 28 ℃ oil bath. The product liquid metal@$SiO_2$ was collected by centrifuging and washing with ethanol and water three time.

**c. PEG and RGD peptides modification of liquid metal@$SiO_2$ nanoparticles:** For PEG modification, methoxy PEG silane (Jenkem Technology Co., Ltd., 25 mg) was added into the 100 mL liquid metal@$SiO_2$ nanoparticles ethanol solution, which was then reacted under magnetic stirring at room temperature for 12 h. For RGD peptide conjugation, the terminal NHS-PEG2000-MAL (Jenkem Technology Co., Ltd.) was used to connect the amino-group-modified liquid metal@$SiO_2$ nanoparticles and the –HS of c(RGDyC) (Chinese Peptide Company) in phosphate buffer solution (PBS) under magnetic stirring for 24 h at room temperature. In detail, liquid metal@$SiO_2$ nanoparticles were first dispersed into ethanol (100 mL), followed by adding APTES (Sigma-Aldrich, 100 μL) for 6 h at 80 °C water bath. Then the obtained $–NH_4$ modified liquid metal@$SiO_2$ nanoparticles after centrifuging and washing were reacted with the terminal NHS-PEG2000-MAL in PBS under magnetic stirring for 24 h at room temperature. Finally, the obtained liquid metal@$SiO_2$-PEG2000-MAL were dissolved in ultrafiltration membranes (cutoff = 4000 kDa) to remove the residual reactants several times and were further redispersed into PBS. The c(RGDyC) was added into the dispersion under magnetic stirring for 24 h at room temperature to trigger the reaction between the thiol group in cysteine and the maleimide of liquid metal@$SiO_2$-PEG2000-MAL, by which liquid metal@$SiO_2$-RGD nanoparticles were synthesized.

## 3. Characterization

Transmission electron microscopy (TEM) photographs were obtained on a JEM-2100F electron microscope (200 kV). X-ray photoelectron spectroscopy (XPS) was conducted on an ESCAlab250 (Thermal Scientific, US). Scanning electron microscopy (SEM) photographs were recorded on a field-emission Magellan 400 microscope (FEI Company, US). Atomic force microscopy (AFM) force–displacement measurement was collected by means of a Veeco DI Nanoscope Multi Mode V system. Zeta potential and dynamic light scattering (DLS) measurements were detected on Zetasizer Nanoseries (Nano ZS90, Malvern Instrument Ltd.). UV-vis-NIR absorption spectra were performed on UV-3600 Shimadzu UV-vis-NIR spectrometer. NIR laser irradiation was produced using an 808 nm high power multimode pump laser (Shanghai

Connect Fiber Optics Company, China). The thermal-field video and temperature detection were recorded on an infrared thermal imaging instrument (FLIR™ A325SC camera, USA). The confocal laser scanning microscopy (CLSM) photographs were acquired in FV1000 (Olympus Company, Japan). Flow cytometry analysis for cell apoptosis and the cellular uptake of the nanosonosensitizers were conducted by BD LSRFortessa. The element quantitative analysis of sample was conducted on inductively coupled plasma-optical emission spectrometry (ICP-OES, Agilent 725, Agilent Technologies, US).

**4. Photothermal performance of liquid metal nanoparticles.**

***a. Calculation of the mass extinction coefficient***

The mass extinction coefficient $\varepsilon(\lambda)$ of the liquid metal nanoparticles was calculated to evaluate the NIR absorption capability of liquid metal nanoparticles, according to the Lambert-Beer Law:

$$A(\lambda) = \varepsilon LC \quad (1)$$

where $\varepsilon$ represents the mass extinction coefficient, $A$ represents the absorbance at a wavelength $\lambda$, $L$ represents path-length (1 cm at here), and $C$ represents the concentration of the liquid metal nanoparticles (in $g \cdot L^{-1}$). The mass extinction coefficient $\varepsilon$ is determined by plotting the slope (in $L \cdot g^{-1}cm^{-1}$) of each linear fit against wavelength. The extinction coefficient ($\varepsilon$) of liquid metal nanoparticles can be calculated to be 10.78 and 9.78 $L \cdot g^{-1}cm^{-1}$ at 808 nm and 1064 nm, respectively (**Figure S7**).

***b. Calculation of the photothermal conversion efficiency***

Following Roper report[1], a continuum energy balance on the whole system is

$$\sum_i m_i C_{p,i} \frac{dT}{dt} = Q_m + Q_{Dis} - Q_{Surr} \quad (2)$$

where $m$ and $C_p$ represent the mass and heat capacity of solvent (water), $T$ represents the solution temperature, $Q_m$ represents the energy input of liquid metal nanoparticles, $Q_{Dis}$ represents the baseline energy input of the sample cell, and $Q_{Surr}$ is the conducting heat away from the system surface by air.

The NIR laser induced source term, $Q_m$, expresses heat dissipated by electron-phonon

relaxation of the plasmon on the liquid metal nanoparticles surface under the irradiation of 808 nm laser:

$$Q_m = I(1 - 10^{-A_\lambda})\eta \quad (3)$$

Where $I$ represents incident energy of laser power (mW), $A_\lambda$ represents the absorbance of the liquid metal nanoparticles at NIR laser wavelength, and $\eta$ represents the photothermal conversion efficiency from NIR laser energy to thermal energy. Besides, $Q_{Dis}$ expresses heat dissipated from light absorbed by the quartz cuvette sample cell, and it was determined independently to be $Q_{Dis} = (5.4 \times 10^{-4})I$ (in mW) using a sample cell containing pure water. $Q_m$ is linear with temperature for the outgoing thermal energy, as the following equation:

$$Q_{surr} = hS(T - T_{Surr}) \quad (4)$$

where $h$ represents heat transfer coefficient, $S$ represents the surface area of the container, and $T_{Surr}$ represents surrounding temperature.

Once the laser power is defined, the heat input $(Q_m + Q_{Dis})$ will be finite. Because the heat output $(Q_{Surr})$ is increased along with the rise of temperature according to the equation (4), the system temperature will reach a maximum when the heat input is equal to heat output:

$$Q_m + Q_{Dis} = Q_{Surr-Max} = hS(T_{Max} - T_{Surr}) \quad (5)$$

where $Q_{Surr-Max}$ represents conducting heat away from the system surface by air when the sample cell reaches the equilibrium temperature. $T_{Max}$ is the equilibrium temperature, representing no heat conduction away from the system surface by air. The photothermal conversion efficiency ($\eta$) can be determined by substituting equation (3) for $Q_m$ into equation (5) and rearranging to yield.

$$\eta = \frac{hS(T_{Max} - T_{Surr}) - Q_{Dis}}{I(1 - 10^{-A_\lambda})} \quad (6)$$

where $A_\lambda$ is the absorbance of liquid metal nanoparticles at NIR laser wavelength (**Fig. S6a**). Therefore, only the $hS$ remains unknown for determining $\eta$.

In order to obtain the $hS$, a dimensionless driving force temperature, $\theta$ is introduced using the maximum system temperature, $T_{Max}$

$$\theta = \frac{T - T_{Surr}}{T_{Max} - T_{Surr}} \quad (7)$$

and a sample system time constant $\tau_s$

$$\tau_s = \frac{\sum_i m_i C_{p,i}}{hS} \quad (8)$$

which is substituted into equation (2) and rearranged to get

$$\frac{d\theta}{dt} = \frac{1}{\tau_s}\left[\frac{Q_m + Q_{Dis}}{hS(T_{Max} - T_{Surr})} - \theta\right] \quad (9)$$

At the cooling period of liquid metal nanoparticles aqueous dispersion, the light radiation ceases, $Q_m + Q_{Dis} = 0$, reducing the following equation

$$dt = -\tau_s \frac{d\theta}{\theta} \quad (10)$$

and integrating, giving the expression

$$t = -\tau_s ln\theta \quad (11)$$

Thus, time constant for heat transfer from the system determined to be 261.19 s of 808 nm and 269.09 s of 1064 nm (**Figure S8e, S6d**). Additionally, the *m* is 0.3 g and the *C* is 4.2 J/g. According to equation (8), the *hS* can be determined. Substituting *hS* into equation (6), the 808 nm laser photothermal conversion efficiency ($\eta$) of liquid metal nanoparticles can be calculated to be 10.21 %. Similarly, the 1064 nm laser photothermal conversion efficiency (η) of liquid metal nanoparticles can be calculated to be 14.12 %.

**5. Photothermal performance of liquid metal@$SiO_2$ nanoparticles.**

***a. Calculation of the mass extinction coefficient***

The calculation details were same as that of liquid metal above. The extinction coefficient ($\varepsilon$) of liquid metal@$SiO_2$ nanoparticles can be calculated to be 20.13 and 16.11 $L \cdot g^{-1}cm^{-1}$ at 808 nm and 1064 nm, respectively (**Figure S7**).

***b. Calculation of the photothermal conversion efficiency***

The calculation details were same as that of liquid metal nanoparticles above. The 808 nm laser photothermal conversion efficiency ($\eta$) of liquid metal@$SiO_2$ nanoparticles can be calculated to be 17.14 %, and the 1064 nm laser photothermal conversion efficiency (η) of liquid metal@$SiO_2$

nanoparticles can be calculated to be 22.43 % (**Figure S8f, 3d**).

**6. Deep-tissue photothermal therapy in NIR-I and NIR-II biowindows.**

The NIR-II biowindow can achieve larger tissue penetration depth in comparison to the commonly studied NIR-I biowindow, because of lower absorption and scattering by tissues in this specific spectrum. We evaluated the tissue-penetration ability of the NIR-I and NIR-II biowindows by detecting the residual laser energy intensity after tissue penetration under 808 and 1064 nm laser irradiation, where chicken breast muscles of varying thickness (0, 2, 4, 6, 8, and 10 mm) were prepared and used as model biological tissues. Then, the deep-tissue photothermal ability in NIR-I and NIR-II biowindows *in vivo* was further assessed by the temperature evaluation in tumors covered with or without tissue after intratumoral injection with 50 μL of a liquid metal@$SiO_2$ dispersion at 200 μg·$mL^{-1}$ upon irradiation with 808 nm and 1064 nm laser (1 W $cm^{-2}$, 5 min).

**7. *In vitro* cytotoxicity against HUVECs (human umbilical vein endothelial cells) and U87 cancer cells.**

HUVECs and U87 human glioblastoma cells (Cell Bank of Shanghai Institutes for Biological Sciences, Chinese Academy of Sciences) were seeded in 96-well culture plates at a density of 3 × $10^3$ cells/well in DMEM medium supplemented with 10 % FBS and 1 % penicillin-streptomycin at 37 °C and 5 % $CO_2$ for 24 h to allow the cells to attach in a humidified incubator. *In vitro* cytotoxicity of liquid metal@$SiO_2$-PEG and liquid metal@$SiO_2$-RGD were evaluated by a standard CCK-8 viability assay (Cell Counting Kit, Dojindo Laboratories, Kumamoto, Japan). Then culture medium above was changed with fresh culture medium containing liquid metal@$SiO_2$-PEG and liquid metal@$SiO_2$-RGD with different Ga concentration (0, 1.6, 3.2, 6.25, 12.5, 25, 50, 100, 200 and 400 μg·$mL^{-1}$). After 24 or 48 h of incubation, CCK-8 assay was used to evaluate the viability of cells (n = 6).

**8. *In vitro* endocytosis and photothermal ablation of cancer cells**

U87 cells were first seeded in 24-well plates at a density of 1 × $10^4$ cells per well in DMEM medium at a 37 °C in the presence of 5 % $CO_2$ for 24 h before treatment. Then, the culture medium was removed, and then liquid metal@$SiO_2$-PEG and liquid metal@$SiO_2$-RGD dispersed in DMEM ([Ga] = 50 μg·$mL^{-1}$) were added into the wells (200 μL per well). After 1 h of incubation,

the culture medium with unbound nanoparticles were removed and cells were rinsed three times with PBS (Runcheng Bio-tech Co., Ltd., Shanghai), and fresh DMEM medium (10 % FBS and 1 % penicillin-streptomycin) was added into the wells. These cells were then irradiated for 5 min under a 1064 nm laser at varied power densities (0, 2.5, 0.5, 1.0, 1.5, and 2.0 $W \cdot cm^{-2}$). In comparison, cells without treated with nanoparticles also accepted irradiation for 5 min. Finally, standard CCK-8 assay was used to evaluate the viability of cells (n = 6).

To investigate the endocytosis of nanoparticles, U87 cells were seeded in CLSM-exclusive culture dishes with a density of $1 \times 10^5$ cells/well and allowed to adhere overnight. Then the cultural medium containing fluorescein isothiocyanate (FITC)-labelled liquid metal@$SiO_2$-PEG and liquid metal@$SiO_2$-RGD at the equivalent Ga dose of 10 $\mu g \cdot mL^{-1}$ were replaced the original medium. For locating the cells, 100 μL of DAPI (Beyotime Biotechnology) was added into dish to stain the cell nuclei for 15 min followed observation with CLSM. For flow cytometry, U87 cells were seeded into six-well microplates at a density of $1 \times 10^5$ cells/plate, and they adhered to the wall of the dish overnight. Then, the culture media were replaced by FITC-labelled liquid metal@$SiO_2$-PEG and liquid metal@$SiO_2$-RGD at the equivalent Ga dose of 10 $\mu g \cdot mL^{-1}$ and then were cultured for1, 2 and 4 h. The cellular uptake of nanoparticles was acquired by flow cytometry equipment.

For examining the photothermal toxicity of nanoparticles *in vitro*, U87 cells were seeded in CLSM-exclusive culture dishes with a density of $1 \times 10^5$ cells/well and allowed to adhere overnight. Then the cultural medium containing liquid metal@$SiO_2$-PEG and liquid metal@$SiO_2$-RGD at the equivalent Ga dose of 10 $\mu g \cdot mL^{-1}$ were replaced the original medium. And then these cells were then irradiated for 5 min under a 1064 nm laser at a power densities of 1.5 $W \cdot cm^{-2}$. In comparison, cells without treated with nanoparticles also accepted irradiation for 5 min. After removal of the DMEM medium, the cells were rinsed with PBS for over three times. U87 cells were incubated with Calcein-AM (100 μL) and PI solution (100 μL) for 15 min. Living cells and dead cells were stained with Calcein-AM (green fluorescence) and PI (red fluorescence) solution, respectively. For flow cytometry, U87 cells were seeded into six-well microplates at a density of $1 \times 10^5$ cells/plate, and they adhered to the wall of the dish overnight. Then, the culture media were replaced by liquid metal@$SiO_2$-PEG and liquid metal@$SiO_2$-RGD at the equivalent Ga dose

of 10 μg·mL$^{-1}$. And then these cells were then irradiated for 5 min under a 1064 nm laser at a power densities of 1.5 W·cm$^{-2}$. In comparison, cells without treated with nanoparticles also accepted irradiation for 5min. After removal of the DMEM medium, the cells were harvested by treatment with 0.25 % trypsin-EDTA solution (Gibco, USA) and stained with annexin V-FITC/PI (Dojindo Molecular Technologies), followed by measurement with BD LSRFortessa.

**9. *In vivo* biocompatibility assay.**

Animal experiment procedures were in agreement with the guidelines of the Regional Ethics Committee for Animal Experiments and the care regulations approved by the administrative committee of laboratory animals of Fudan University. Healthy female Kunming mice (~ 22 g) were obtained and raised at Laboratory Animal Center, Shanghai Medical College of Fudan University. 28 SBF-level female Kunming mice (4 weeks old) were divided into four groups to be injected with liquid metal@SiO2-RGD at different Ga dose (0, 2.5, 5, and 10 mg·kg$^{-1}$). After a whole month's recording of the body weight of mice every 2 days, they were sacrificed and their organs (heart, liver, spleen, lung, and kidney) and blood samples were collected for evaluation, including H&E staining and various blood-index monitoring.

**10. Pharmacokinetics, biodistribution and metabolism studies.**

To develop the tumor model, U87 cells (1 × 10$^6$ cell/site) suspended in 150 μL PBS solution were injected into the back of mice. In pharmacokinetic experiments, U87 tumor-bearing mice were intravenously administered with liquid metal@$SiO_2$-RGD (10 mg·kg$^{-1}$) in PBS (n = 3). The 10 μL of blood was collected at varied time intervals (2 min, 5 min, 10 min, 0.5 h, 1 h, 2 h, 4 h, 8 h and 24 h) after injection. The quantitative analysis of Ga element was measured by ICP-OES. The *in vivo* blood terminal half-life of liquid metal@$SiO_2$-RGD was determined by a double-component pharmacokinetic model.

Biodistribution of liquid metal@$SiO_2$-RGD in tumor and other organs was performed in U87 tumor-bearing mice (n = 3). U87 tumor-bearing mice were intravenously administered with liquid metal@$SiO_2$-RGD (10 mg·kg$^{-1}$) in PBS. Mice were dissected at predesignated time intervals (4, 24, and 48 h). Dissected organs were weighed, homogenized, and treated with strong acid. The

liquid metal@$SiO_2$-RGD distributions in different tissues were calculated as the percentage of injected Ga dose per gram of tissue.

To investigate the metabolism process of liquid metal@$SiO_2$-RGD, liquid metal@$SiO_2$-RGD nanoparticles in PBS (10 $mg \cdot kg^{-1}$ per mouse) were intravenously injected into the U87 tumor-bearing mice. The urine and faces were collected at different time intervals (2, 6, 12, 24, 36, 48 and 7 d). The Ga contents in urine and faeces were quantitatively determined by ICP-OES.

**11. *In vivo* photothermal therapy in NIR-II biowindow.**

The 5-week old female Balb/c nude mice (~ 13 g) were obtained and raised at Laboratory Animal Center, Shanghai Medical College of Fudan University. To develop the tumor model, U87 cells ($1 \times 10^6$ cell/site) suspended in 100 μL PBS solution were injected into the back of mice. *In vivo* photothermal therapy by intravenous administration was performed when the tumors volume reached ~150 $mm^3$. All mice were anesthetized before NIR-II laser irradiation. The measurement of the tumors volume was conducted by a digital caliper every two days during half a month after the corresponding experiments. The tumor volume was measured according to the following formula: tumor volume = (tumor length) × $(\text{tumor width})^2$ /2. The tumors were dissected after the corresponding treatments and fixed in a 10 % formalin. Thereafter, the tumor issues were sectioned into slices and stained with H&E, TUNEL and Ki-67 for histological analysis.

## *Part B. Supplementary figures and discussions*

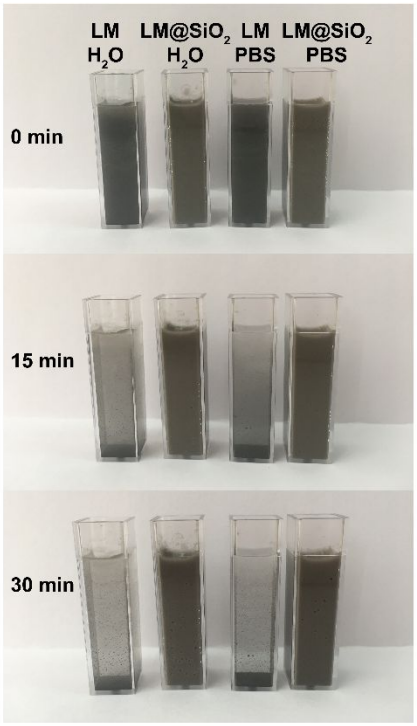


**Figure S1**. Dispersing stabilities of the constructed liquid metal and liquid metal@$SiO_2$ nanoparticles in water and phosphate buffer solution (PBS).

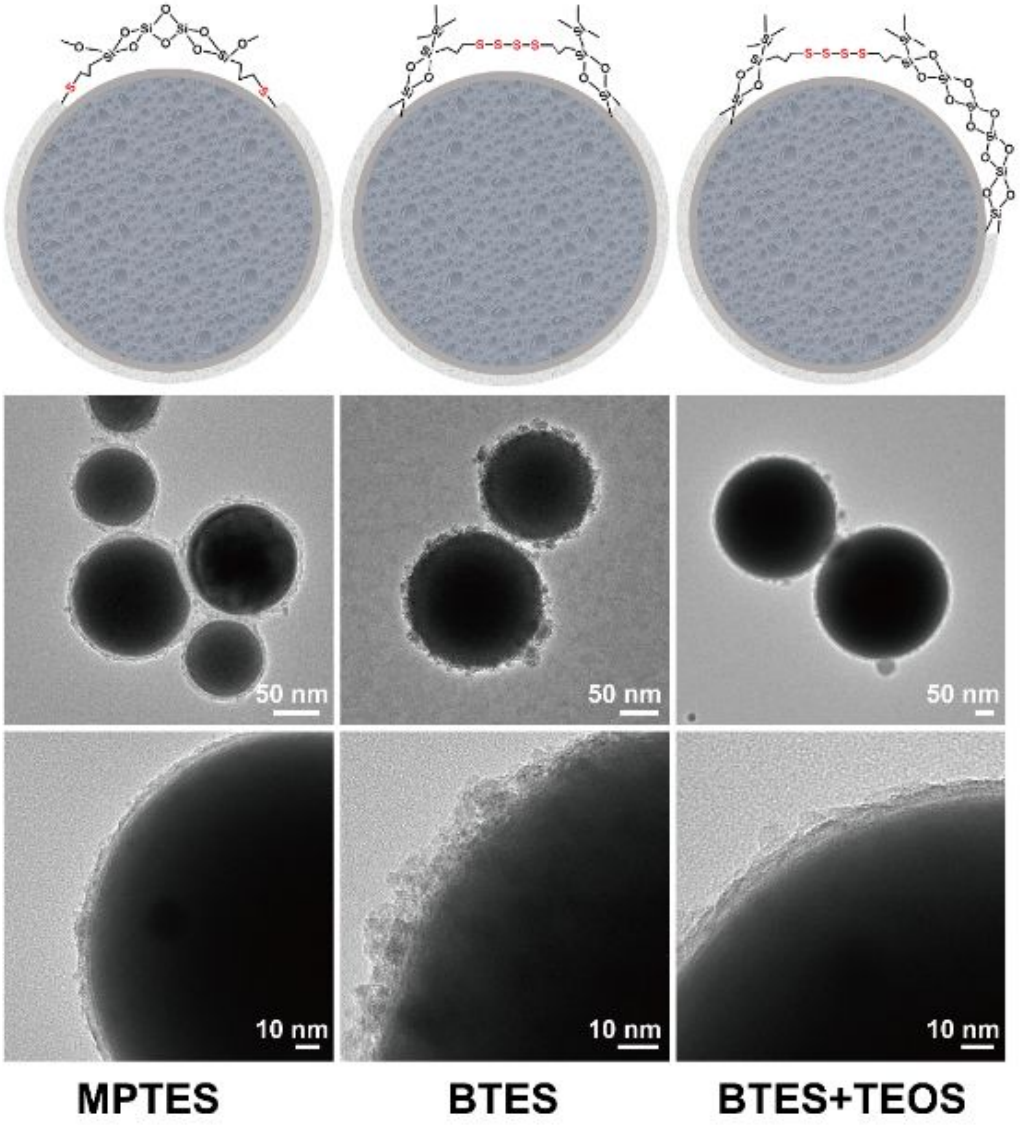


**Figure S2.** Schemes of the layer structures and corresponding TEM images of the protective layer by depositing three other silicon sources, including MPTES, BTES and BTES + TEOS.

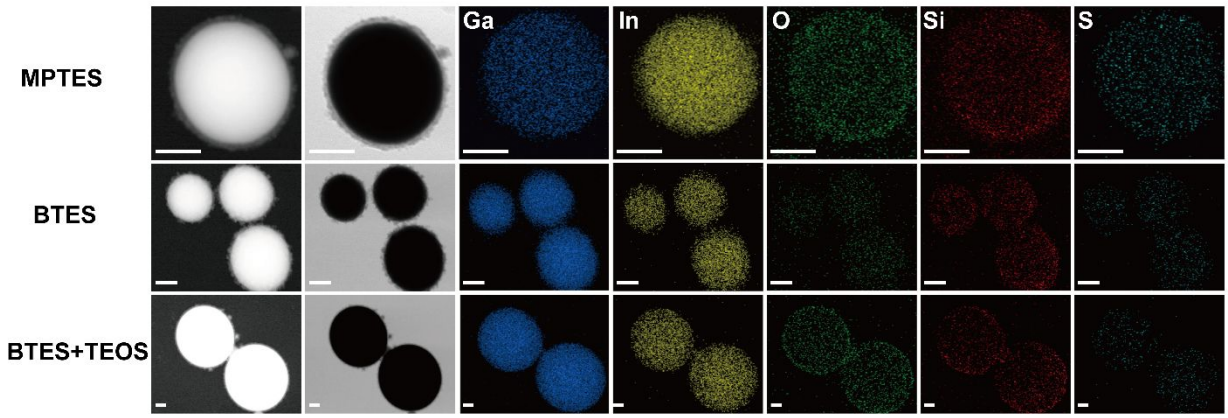


**Figure S3**. Element mapping of the protective coatings by depositing three other silicon sources. Scale bar = 50 nm.

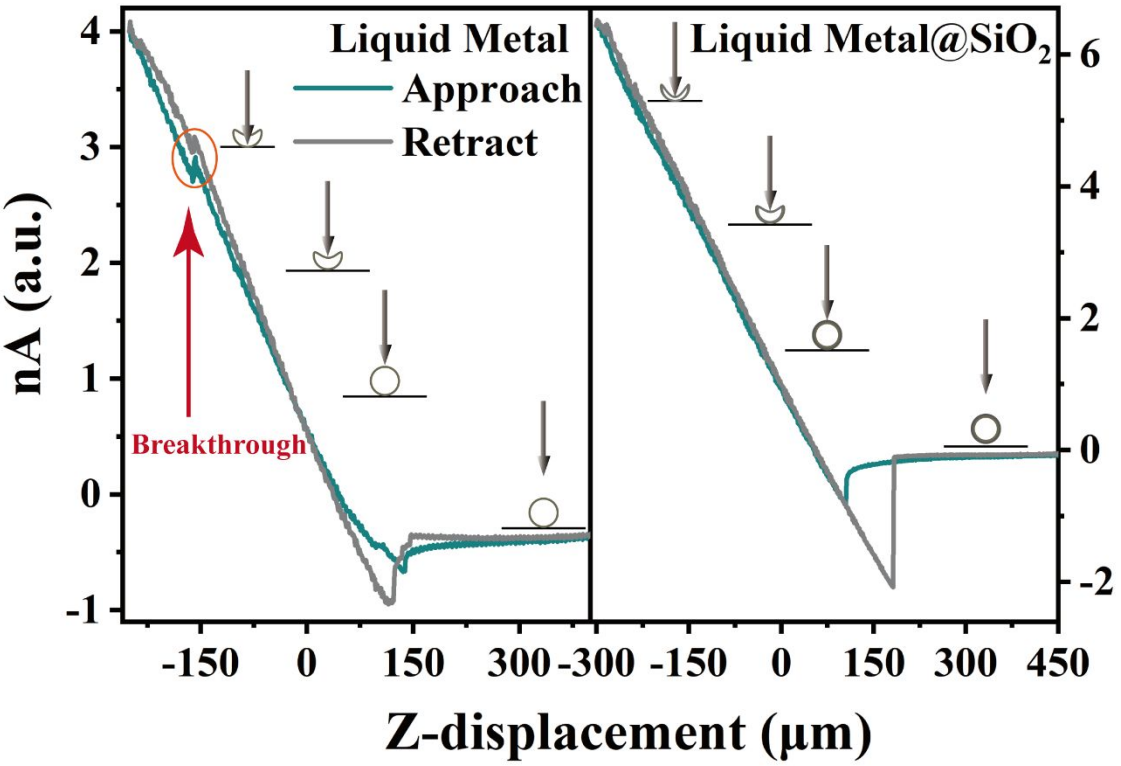


**Figure S4.** Force–displacement curve obtained for single liquid metal nanoparticle and liquid metal@$SiO_2$ nanoparticle; the cyan line tracks the approaching trajectory between the AFM tip and the particle, while the gray line tracks the retraction trajectory of the AFM tip from the particle; the circled kink means the breakthrough of the liquid metal nanoparticle.

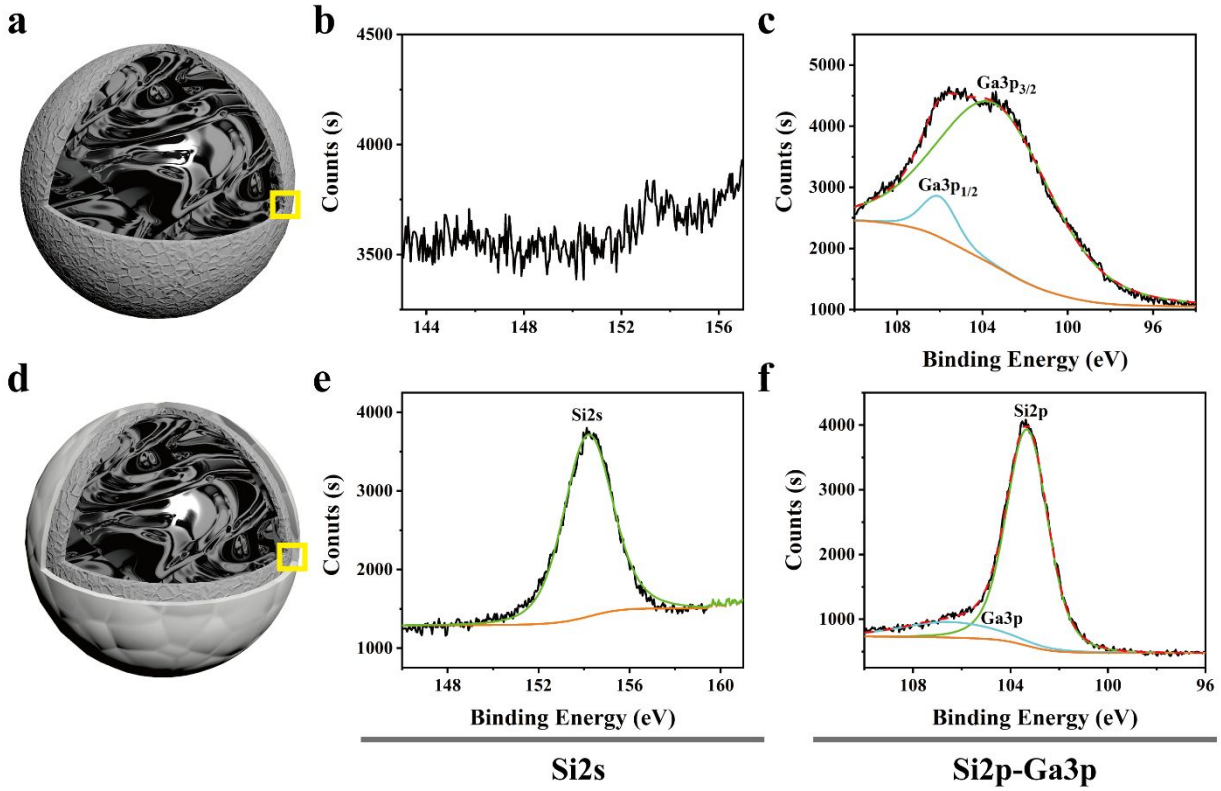


**Figure S5. XPS of liquid metal nanoparticles and liquid metal@$SiO_2$ nanosystems.** (a, d) Schematic illustration, (b, e) Si 2s spectra and (c, f) Si 2p - Ga 3p spectra of liquid metal nanoparticles (a - c) and liquid metal@$SiO_2$ nanoparticles (d - f).

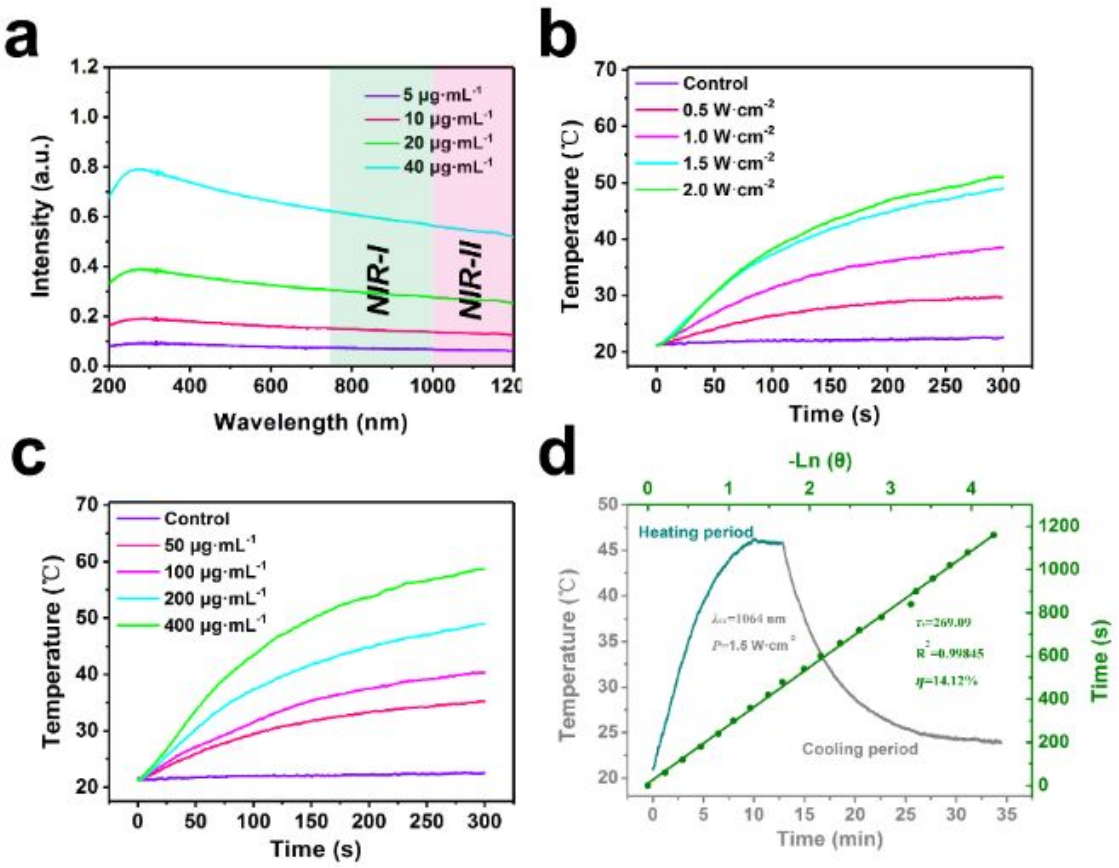


**Figure S6. Photothermal-conversion performance of naked liquid metal nanoparticle in NIR-II window.** (a) Vis-NIR absorbance spectra of liquid metal-dispersed aqueous suspensions at varied concentration (5, 10, 20 and 40 μg·mL$^{-1}$). (b, c) Photothermal heating curves of liquid metal@$SiO_2$-dispersed aqueous suspensions at varied power densities (200 μg·mL$^{-1}$; 0.5, 1.0, 1. 5 and 2.0 W·cm$^{-2}$) and concentration (1.5 W·cm$^{-2}$; 50, 100, 200 and 400 μg·mL$^{-1}$). (d) Calculation of the photothermal-conversion efficiency.

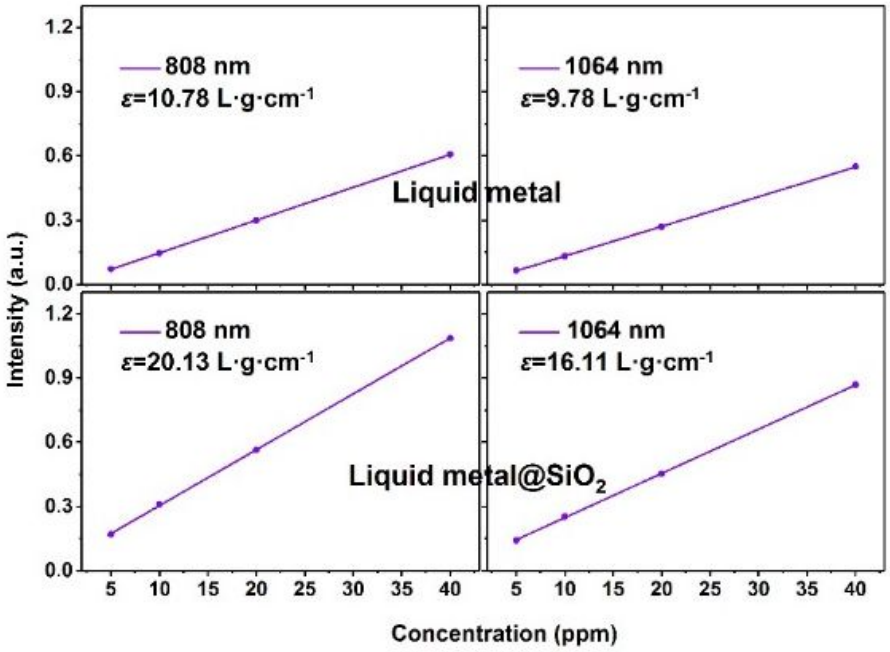


**Figure S7.** Mass extinction coefficients of liquid metal and liquid metal@$SiO_2$ at 808 nm and 1064 nm.

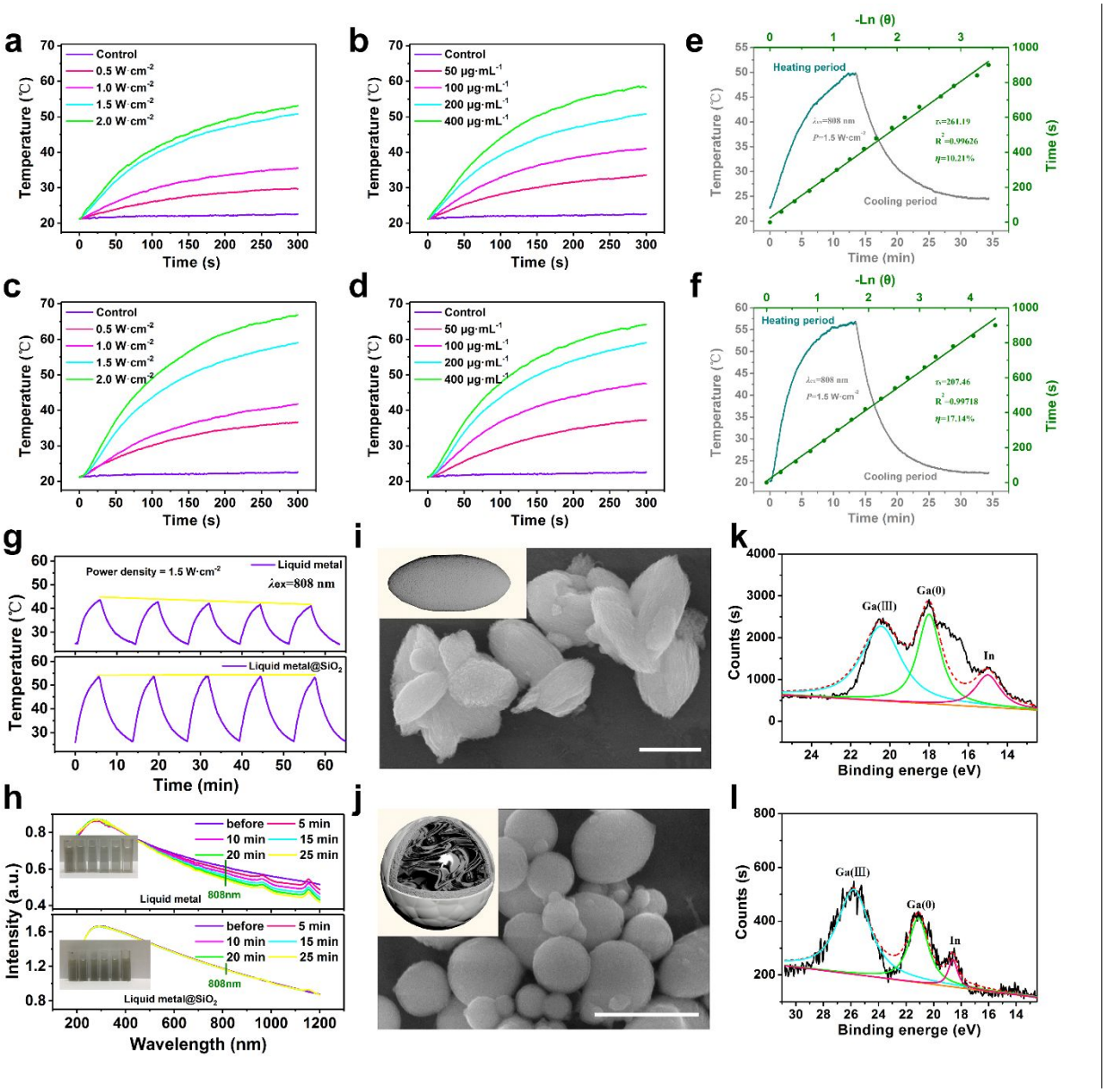


**Figure S8. Photothermal-conversion performances of liquid metal@$SiO_2$ nanoparticles and stability compared with bare liquid metal nanoparticles in NIR-I window.** (a - d) Photothermal-heating curves of liquid metal-dispersed (a, b) and liquid metal@$SiO_2$-dispersed (c, d) aqueous suspensions at varied power densities (0.5, 1.0, 1.5 and 2.0 W·$cm^{-2}$ at 200 μg·$mL^{-1}$) and concentrations (50, 100, 200 and 400 μg·$mL^{-1}$ at 1.5 W·$cm^{-2}$). (e - f) Calculation of the photothermal-conversion efficiencies of liquid metal (e) and liquid metal@$SiO_2$ (f). (g, h) Heating curves (g), and vis-NIR absorbance spectra (h) of the aqueous suspension of liquid metal with or without protective $SiO_2$ coating for five laser on/off cycles (200 μg·$mL^{-1}$, 1.5 W·$cm^{-2}$), and left inset are digital photo of samples after each duration. (i, j) SEM image and (k, l) XPS spectra of

liquid metal nanoparticles (i, k) and liquid metal@$SiO_2$ nanoparticles (j, l) after irradiation. Scale bar = 200 nm.

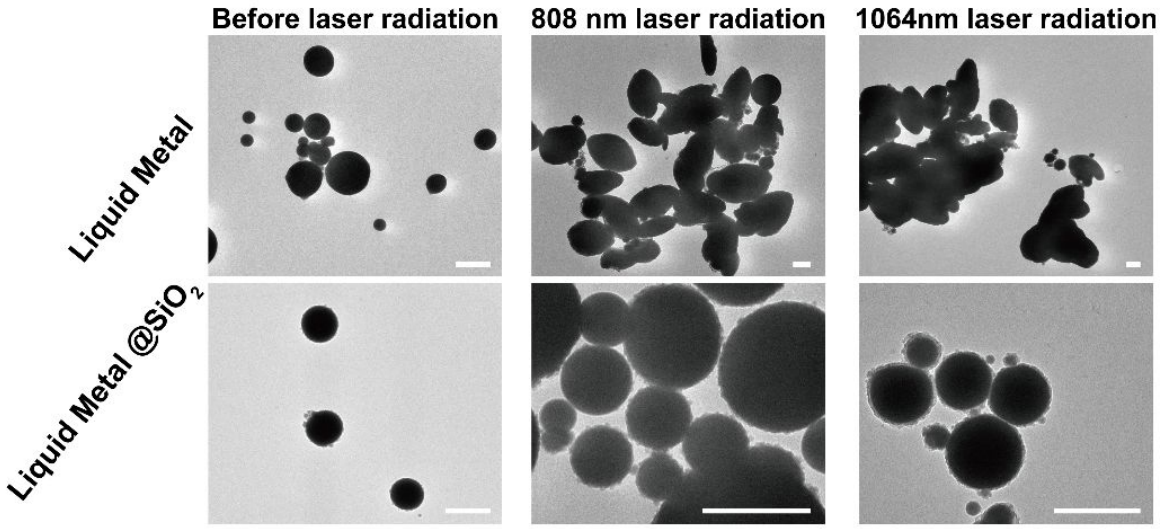


**Figure S9.** TEM images of liquid metal and liquid metal@$SiO_2$ before and after irradiation. Scale bar = 200 nm.

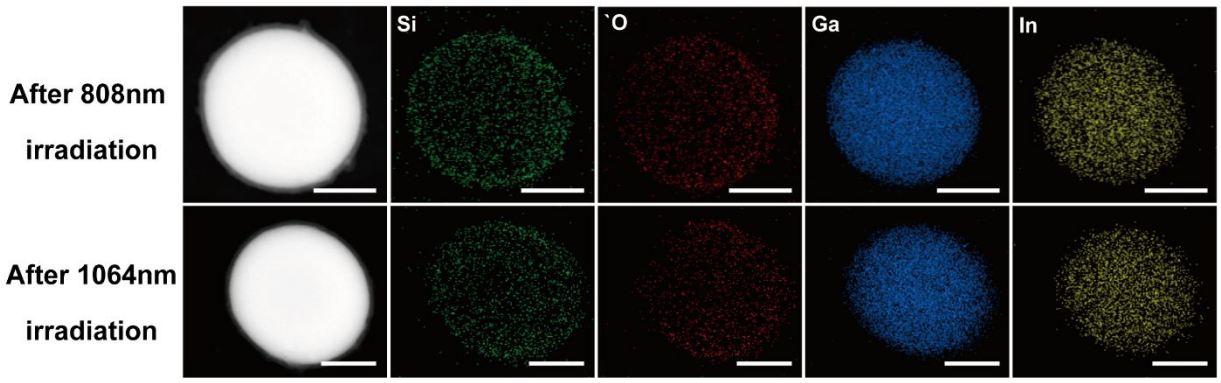


**Figure S10.** Elements mapping of liquid metal@$SiO_2$ after laser irradiation. Scale bar = 100 nm.

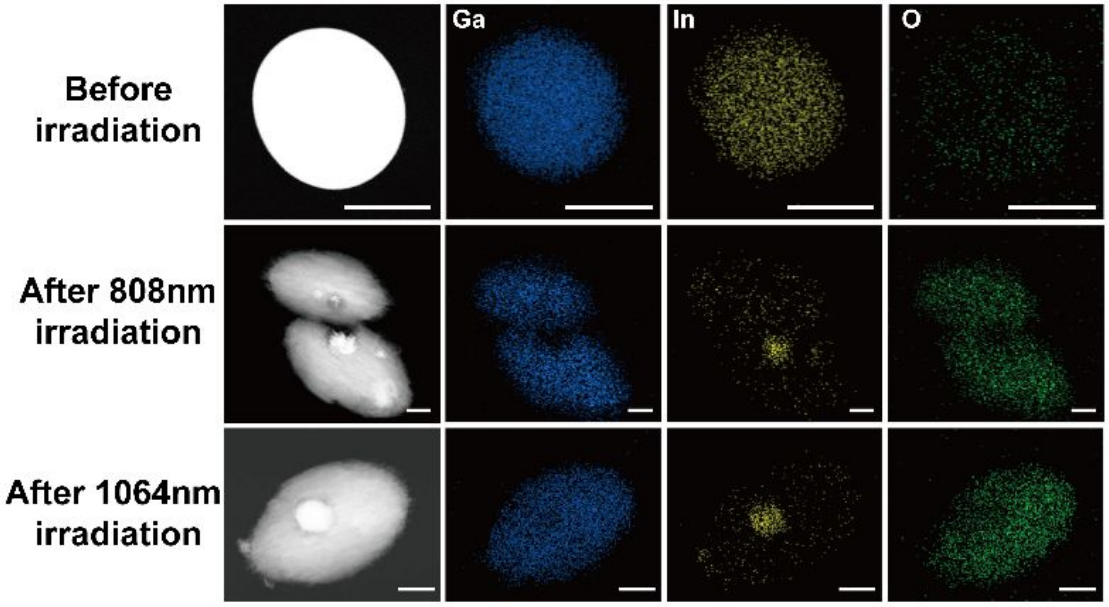


**Figure S11.** Elements mapping of liquid metal before and after laser irradiation. Scale bar = 100 nm.

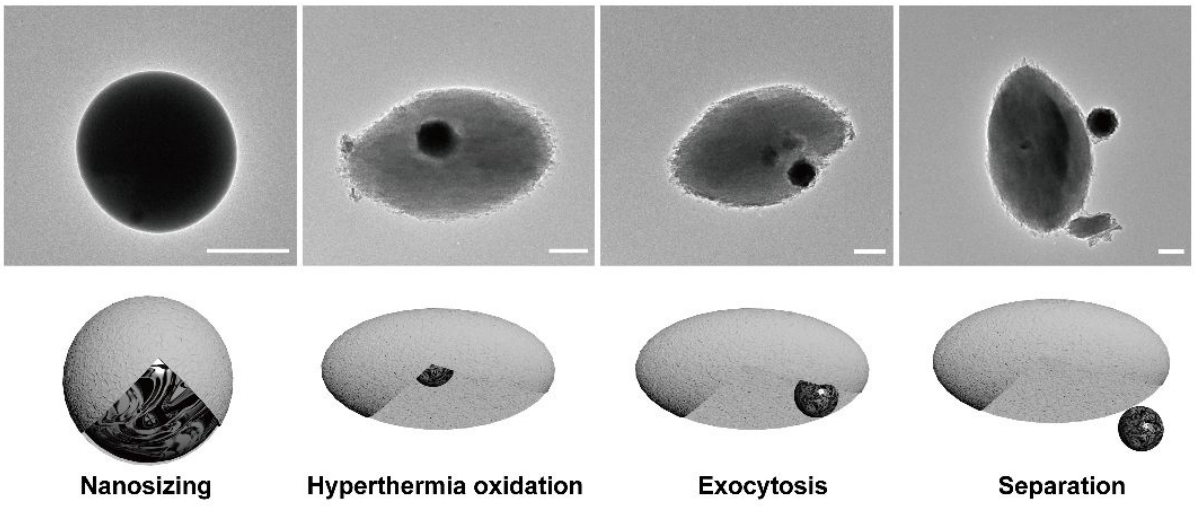


**Figure S12.** Several morphologies in liquid metal-deformed samples and the speculation of liquid metal in the process of deformation during irradiation. Scale bar = 100 nm.

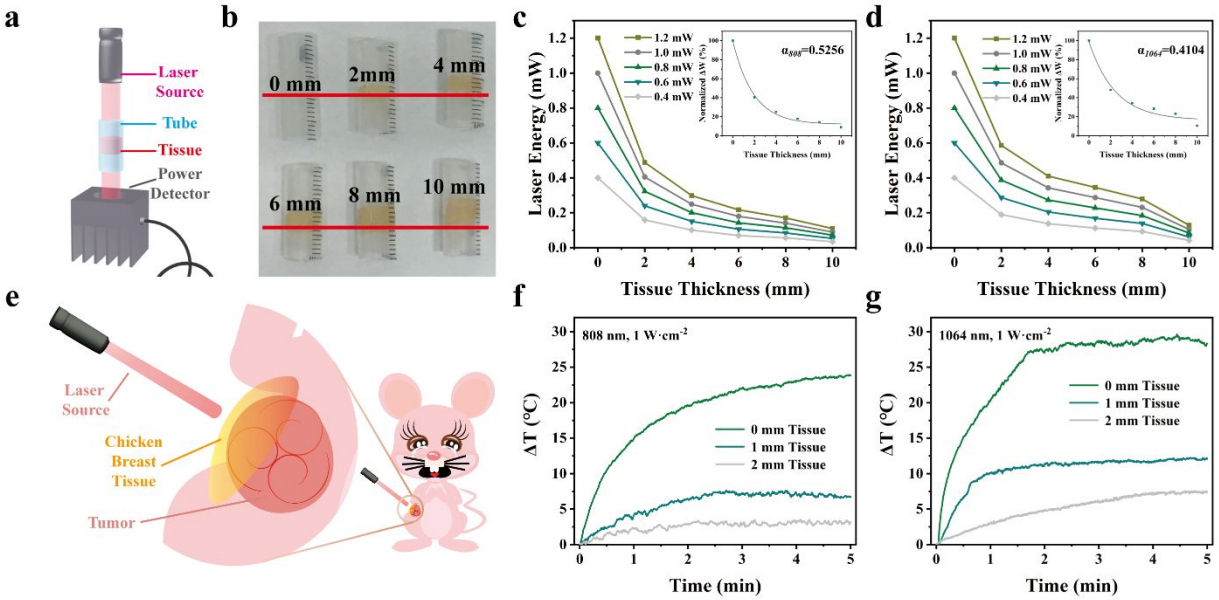


**Figure S13. Evaluation of *in vitro* and *in vivo* tissue-penetration depth for NIR-I and NIR-II photothermal conversion.** (a) Schematic diagram and equipment for detecting tissue-penetration capability of NIR laser at 808 and 1064 nm. (b) Different thicknesses (0, 2, 4, 6, 8, and 10 mm) of chicken breast tissues fixed in transparent pipes. (c) Energy intensities of NIR-I laser (808 nm) penetrating through tissues of different thicknesses. Inset: Normalized penetrated NIR-I energy through tissues of different depths. $\alpha_{808}$: the attenuation coefficient of 808 nm NIR-I laser. (d) Energy intensities of NIR-II laser (1064 nm) penetrating through tissues of different thicknesses. Inset: Normalized NIR-II energy penetrating through tissues of different depths. $\alpha_{1064}$: the attenuation coefficient of 1064 nm NIR-II laser. Schematic illustration (e) and the *in vivo* temperature evaluations in tumor covered with the tissue after intratumoral injection with 50 μL of a liquid metal@$SiO_2$ dispersion at 200 μg·$mL^{-1}$ upon irradiation by (f) 808 nm and (g) 1064 nm laser (1 W·$cm^{-2}$, 5 min).

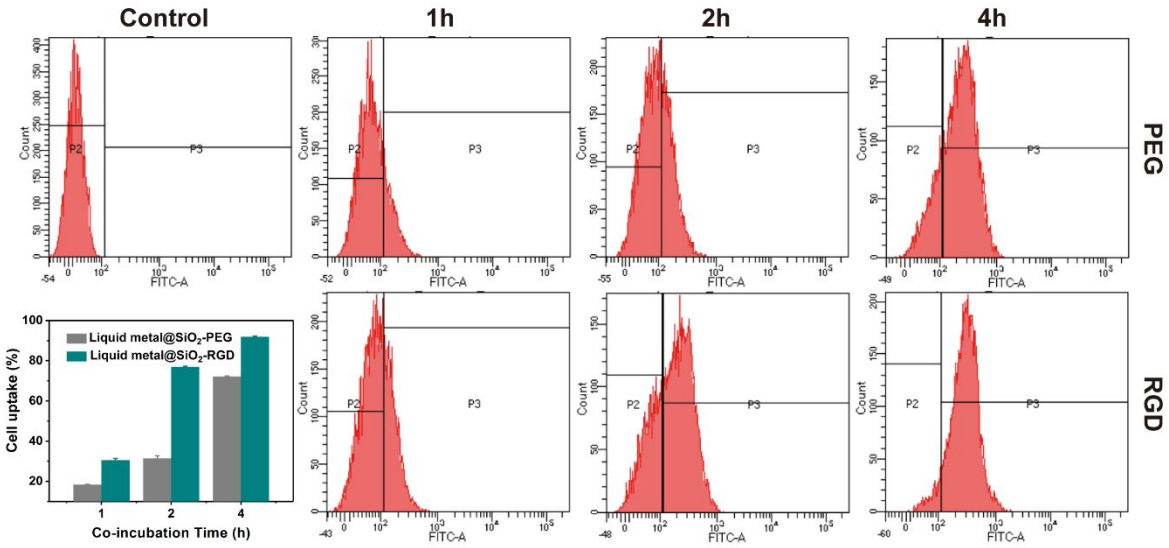


**Figure S14.** Flow cytometry analysis of cellular endocytosis of liquid metal@$SiO_2$ with or without RGD-targeting modification after incubation for different durations.

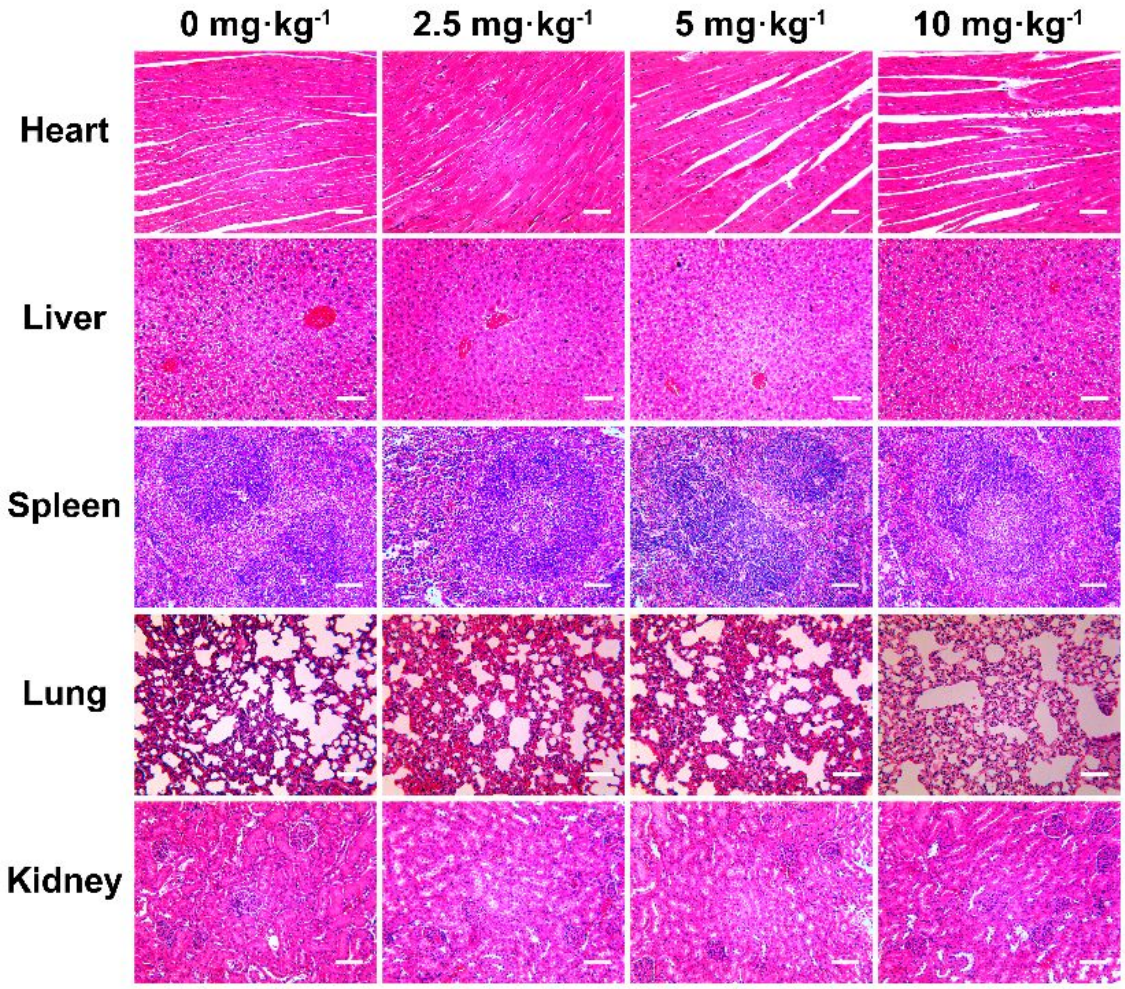


**Figure S15.** Histological sections obtained from heart, liver, spleen, lung, and kidney of different Ga doses of liquid metal@$SiO_2$-RGD treated the mice sacrificed 30 days post-injection. Scale bar = 200 μm.

***Part C. Supplementary tables***

**Table S1**. Energy dispersive X-ray spectroscopy of liquid metal and liquid metal functioned with protective coatings by depositing different silicon sources.

| Samples | Ga | In | O | Si | S |
|---|---|---|---|---|---|
| **Liquid metal** | **51.56 %** | **25.39 %** | **23.05 %** | **—** | **—** |
| **TEOS** | **56.79 %** | **27.37 %** | **12.67 %** | **3.17 %** | **—** |
| **MPTES** | **53.32 %** | **33.59 %** | **9.8 %** | **2.66 %** | **0.63 %** |
| **BTES** | **56.52 %** | **31.46 %** | **10.32 %** | **1.25 %** | **0.45 %** |
| **BTES+TEOS** | **59.53 %** | **30.77 %** | **7.04 %** | **2.32 %** | **0.34 %** |

**Table S2**. Atomic ratios of liquid metal and liquid metal @$SiO_2$ before and after laser irradiation from XPS data.

| | Liquid Metal | after 808 nm | after 1064 nm | Liquid Metal@$SiO_2$ | after 808 nm | after 1064 nm |
|---|---|---|---|---|---|---|
| **Ga** | **35.84%** | **28.59%** | **26.80%** | **1.36%** | **1.48%** | **0.99%** |
| **In** | **7.69%** | **2.07%** | **1.09%** | **0.11%** | **0.06%** | **0.04%** |
| **O** | **56.47%** | **69.34%** | **72.09%** | **65.61%** | **65.85%** | **65.19%** |
| **Si** | —— | —— | —— | **32.92%** | **32.61%** | **33.33%** |

***Part D. References***

(1) Roper, D. K.; Ahn, W.; Hoepfner, M., *J. Phy. Chem. C,* **2007,** 111, 3636-3641.